Lead-related quantum emitters in diamond

Matthew E. Trusheim, Noel H. Wan, Kevin C. Chen, Christopher J. Ciccarino, Johannes Flick, Ravishankar Sundararaman, Girish Malladi, Eric Bersin, Michael Walsh, Benjamin Lienhard, Hassaram Bakhru, Prineha Narang, and Dirk Englund

Phys. Rev. B **99**, 075430 — Published 21 February 2019

DOI: 10.1103/PhysRevB.99.075430

Lead-Related Quantum Emitters in Diamond

Matthew E. Trusheim[1,,†], Noel H. Wan[1,*], Kevin C. Chen[1,*], Christopher J. Ciccarino[2,3], Johannes Flick[2], Ravishankar Sundararaman[4], Girish Malladi[5], Eric Bersin[1], Michael Walsh[1], Benjamin Lienhard[1], Hassaram Bakhru[5], Prineha Narang[2], and Dirk Englund[1]*

Affiliations

[1]Department of Electrical Engineering and Computer Science, Massachusetts Institute of Technology, Cambridge, Massachusetts 02139, USA
[2]John A. Paulson School of Engineering and Applied Sciences, Harvard University, Cambridge, Massachusetts 02138, USA
[3]Department of Chemistry and Chemical Biology, Harvard University, Cambridge, Massachusetts, 02138, USA
[4]Department of Materials Science and Engineering, Rensselaer Polytechnic Institute, Troy, NY, United States
[5]College of Nanoscale Science and Engineering, Suny Poly, 257 Fuller Road, Albany, NY 12203, United States

[†]mtrush@mit.edu

*These authors contributed equally to this work

Abstract

We report on quantum emission from Pb-related color centers in diamond following ion implantation and high temperature vacuum annealing. First-principles calculations predict a negatively-charged Pb-vacancy center in a split-vacancy configuration, with a zero-phonon transition around 2.4 eV. Cryogenic photoluminescence measurements performed on emitters in nanofabricated pillars reveal several transitions, including a prominent doublet near 520 nm. The splitting of this doublet, 5.7 THz, exceeds that reported for other group-IV centers. These observations are consistent with the PbV center, which is expected to have the combination of narrow optical transitions and stable spin states, making it a promising system for quantum network nodes.

Introduction

Quantum emitters in diamond and other wide-bandgap materials are promising systems for quantum information processing[1,2]. In particular, the nitrogen-vacancy center in diamond (NV) has been shown to possess both long-lived spin states[3] and a high-fidelity spin-photon interface[4], enabling quantum networking protocols[5]. However, the NV's optical properties remain a challenge: only a small fraction of the fluorescence branches into the coherent zero-phonon line (ZPL), as given by a Debye-Waller factor (DWF) of ~0.03[6], and spectral diffusion broadens the ZPL significantly in nanophotonic devices[7,8,9].

These limitations have spurred a search for alternative quantum emitters. These include the negatively-charged silicon-vacancy (SiV^-) center, which has a larger DWF ~0.8[10] and stable optical transitions even in nanophotonic structures[11] due to its crystallographic inversion symmetry[12,13]. To achieve long spin coherence in SiV^- centers, it is necessary to cool the sample

such that $k_BT << h\Delta_{GS}$, where Δ_{GS} is the ground state orbital splitting, to reduce phonon absorption in the ground state manifold. For the SiV^- defect, with Δ_{GS} = 50 GHz, temperatures below 500 mK are required to achieve millisecond coherence times[14]. Heavier group IV-vacancy centers are expected to share the favorable inversion symmetry, yielding narrow optical lines, but with larger ground state orbital splittings that could increase spin coherence times[15]. In previous reports of group IV defects, the germanium-vacancy has been shown to have narrow optical lines[16,17] and Δ_{GS} = 150 GHz , and the tin-vacancy has been observed[18,19] with Δ_{GS} = 850 Δ_{GS} effectively relaxes the temperature requirement for achieving long coherence times, motivating the search for defects with heavier elements.

Here we report the observation of color centers associated with the heaviest naturally-occurring group IV element, lead (Pb). Our first-principles density functional theory (DFT) calculations predict a stable negatively-charged Pb-vacancy (PbV) color center in the diamond lattice. We created Pb-related color centers through an ion implantation and annealing process and characterized them through photoluminescence spectroscopy at cryogenic temperatures. As discussed below, we find good agreement between DFT predictions of the transition energies and our spectroscopy.

First Principles Calculations of Defects and Spectra

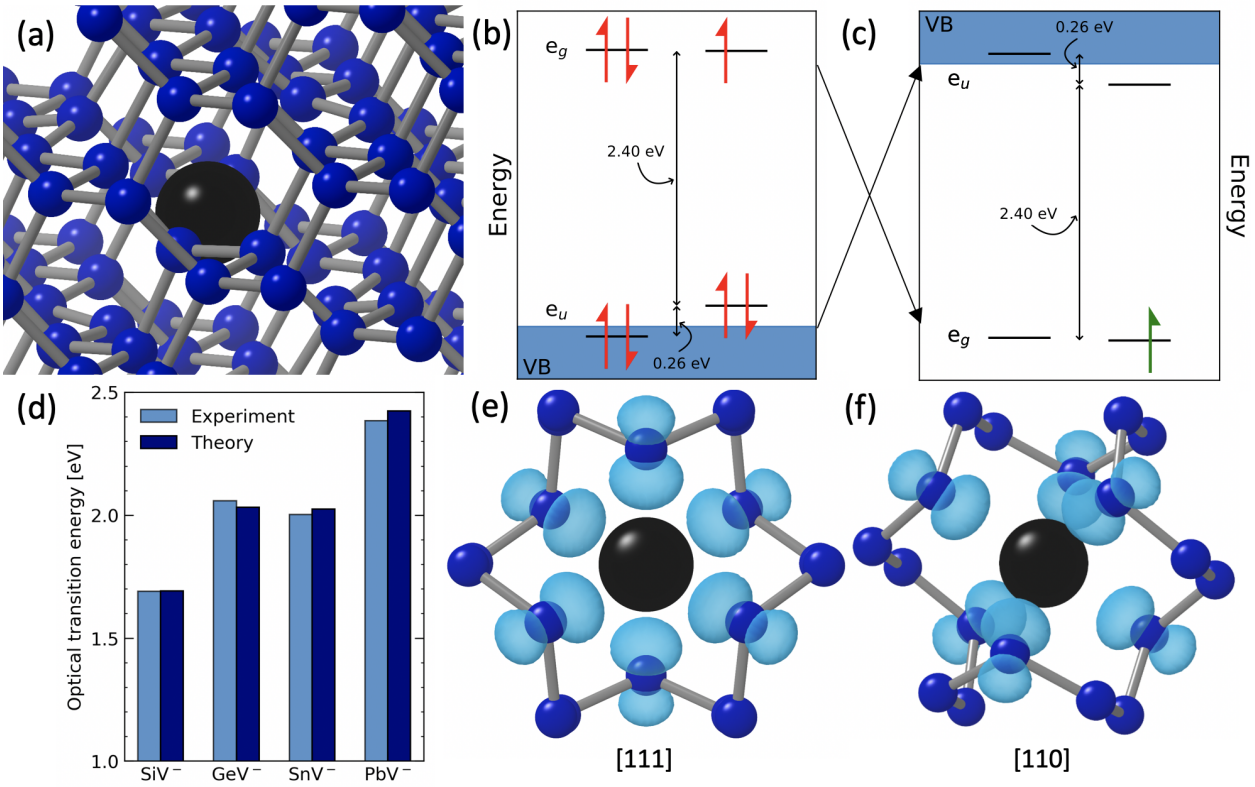

Figure 1: PbV calculations from first principles. (a) A Pb atom (black) in a split-vacancy configuration within the diamond lattice (blue spheres: carbon atoms). (b) The electron orbital structure of the PbV defect in a negative charge state. Both the e_u and e_g orbitals are split as a result of strong spin-orbit coupling. The energy difference between the e_u and e_g orbitals have been adjusted by the HSE-calculated ZPL energy. (c) The same PbV orbital structure from a

hole perspective. (d) Comparison of predicted optical transition energies of group-IV defects with experimental data[18,20,21] and present work. (e,f) Electron density associated with the negatively-charged PbV viewed from the [111] and [110] axes, respectively. The density is primarily distributed to the six nearby carbon atoms of the diamond lattice.

First, we performed first-principles simulations of the PbV defect using the Quantum Espresso[22,23] software package. We use a 512 atom supercell with gamma-point integration and norm-conserving pseudopotentials[24] with a 40 hartree plane-wave energy cutoff. Structural relaxations were performed with the PBE exchange-correlation functional[25], where we find the defect to be stable in the split-vacancy configuration, described by the inversion-symmetric D_{3d} point group. The predicted orbital structure, which is composed of two pairs of orbitals, e_u and e_g, is shown in Figure 1b. In the inversion-symmetric configuration, both of these orbitals are energetically degenerate, but they split as a result of spin-orbit coupling, which has contributed significantly in lighter group-IV defects[17,26]. To determine the zero phonon line, we employ the HSE06 hybrid functional[27] within Quantum Espresso in conjunction with constrained-occupation DFT (i.e., ΔSCF[28]) to capture the ZPL, which we find to be 2.40 eV (517 nm), in excellent agreement with Reference 15. These simulations use the PBE-optimized geometries for the ground and excited states are used to determine the ZPL for the PbV^- as well as the other negatively-charged group-IV defects. In each of these cases, we determined the optimized geometry by relaxing the atoms in the structure until a tight force convergence criterion of 10^{-6} ev/Å was met. The resulting HSE ZPL energies are within all 3% of experiment, suggesting very good agreement, as seen in Fig 1d.

The seven-electron orbital configuration of the PbV is most simply described in terms of a single-hole picture. This is schematically presented in Figure 1c, where we follow convention and flip the energy axis. From this perspective, the potential transitions of the hole from excited states (e_u orbitals) to ground states (e_g orbitals) correspond to optical emission at different energies. The difference in energy between e_g orbitals is the ground-state splitting Δ_{GS}, while the splitting between e_u orbitals is the excited state splitting Δ_{ES}, consistent with previous convention[26]. We determine these energies by including spin-orbit coupling in our calculations at the PBE level with relativistic norm-conserving pseudopotentials. This has been found to be in agreement with HSE-based spin-orbit splitting for the ground state[15]. Both the ground and excited state splittings increase with the size of the group-IV atom, with the PbV having the Δ_{GS}= 30 meV, Δ_{ES}= 260 meV. Note that our calculations do not account for the spin-orbit quenching phenomena which can arise from the dynamic Jahn-Teller effect via the Ham reduction factor[29]; this would lower the magnitude of the ground and excited state splittings.

Figure 2: Calculated relative emission intensity from first-principles. Dipole matrix elements between each PbV orbital are calculated and compared for different temperatures using JDFTx.(a) Predicted emission at zero temperature. The emitting transitions originate from the lower-energy e_u orbital (i.e., channels D and C), under the assumption that thermal equilibrium

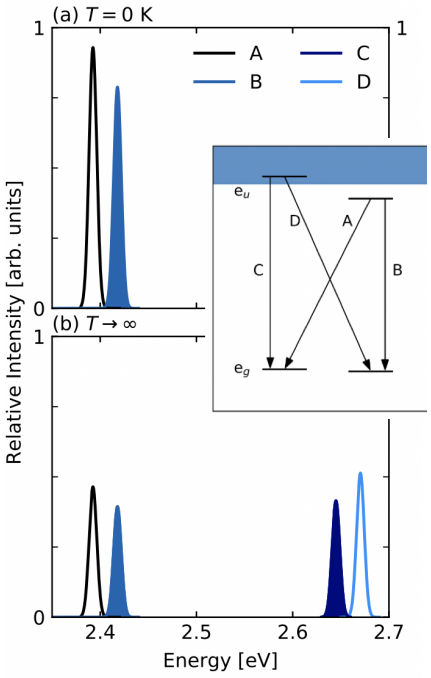

is achieved prior to emission[30]. In the high temperature limit presented in panel (b), transitions to all four orbitals are thermodynamically allowed, resulting in a four-peak structure. Filled peaks indicate emission polarized along the PbV [111] direction (transitions B, C), while unfilled peaks are polarized perpendicular to the defect axis. We note that the energy values are corrected according to the HSE-calculated ZPL energy.

We next used the JDFTx[31] software package to predict the strengths of the optical transitions via Fermi's Golden rule. We calculate the momentum matrix elements $\langle \psi_n | \vec{p} | \psi_{n'} \rangle$ for PbV states n and n' as input to Fermi's Golden Rule. Figure 2 presents the relative coupling strengths of the four zero-phonon transitions A, B, C, and D at T = 0 and T →∞. Electron-phonon interactions[32,33] would introduce additional spectral features and broaden the linewidths of each transition. There are only two peaks at low temperatures because we assume that the e_u orbitals reach thermal equilibrium before emission[30]. Thus, de-excitation of an excited hole would only occur out of the lower-energy e_u orbital, which is located within the band gap. To model emission at elevated temperatures, we introduce a Boltzmann distribution, which in the high temperature limit allows all four orbitals to be equally occupied. As a result, four peaks are expected in the emission spectrum (Figure 2b). From these calculations, we also obtain the emission polarization. As shown, two of the four transitions (B and C) are polarized along the PbV [111] axis. The two other emission channels (A and D) have polarization perpendicular to the defect axis. We observed this polarization trend for each of the lighter group-IV defects as well.

Experiment

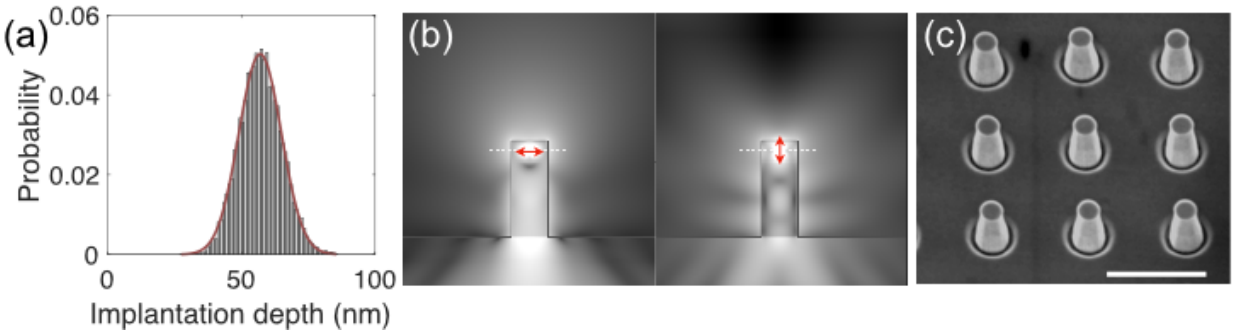

Figure 3: Sample preparation. (a) Simulated Pb ion probability distribution, centered around (58 ±8) nm in depth. (b) Field profile of an emitter in a nanopillar with a diameter of 225 nm and height of 600 nm. Red arrow: polarization of a dipole emitter. Dashed white line: predicted depth of Pb-related emitters (c) Scanning electron micrograph of the fabricated nanopillar array. Scale bar: 1 μm.

We prepared the sample by ion implantation into commercially-available type-IIa diamond (< 5 ppb [N],[B]; Element6) at an energy of 350 keV and a dose of 10^9 Pb cm^{-2} (Varian Extrion 10 - 400 keV ion implanter). Stopping range of ions in matter (SRIM) calculations[34] (Figure 3a) predict that this implantation produces a Pb layer with a mean depth of (58 ± 8) nm. Each implanted Pb ion is predicted to produce ~ 2000 vacancies during implantation; although an order of magnitude more than expected for other species such as nitrogen, the predicted peak vacancy density of ~10^{17} cm^{-3} is still well below the graphitization damage threshold for diamond[35]. Following implantation, we annealed the sample under high vacuum (< 10^{-7} mbar) at 1200 °C for two hours and cleaned it in boiling acid[36].

The resulting sample had a density of emitters too high to spatially isolate a single color center[36]. To isolate single Pb-related emitters, we fabricated nanopillars into the diamond using a combination of electron beam lithography and reactive ion etching[36] (Figure 3b,c). The pillar diameters varied from 150 to 325 nm, with a height of 670 nm. For collection using an NA = 0.9 objective, finite-difference time-domain (FDTD) calculations indicate that the pillars additionally provide a 5 to 10X fluorescence collection efficiency enhancement for an emitter located at a depth of 60 nm as compared to that in an unpatterned diamond. The scanning electron micrograph in Figure 3c shows the set of nanopillars with a diameter of 225 nm that are primarily investigated in this work.

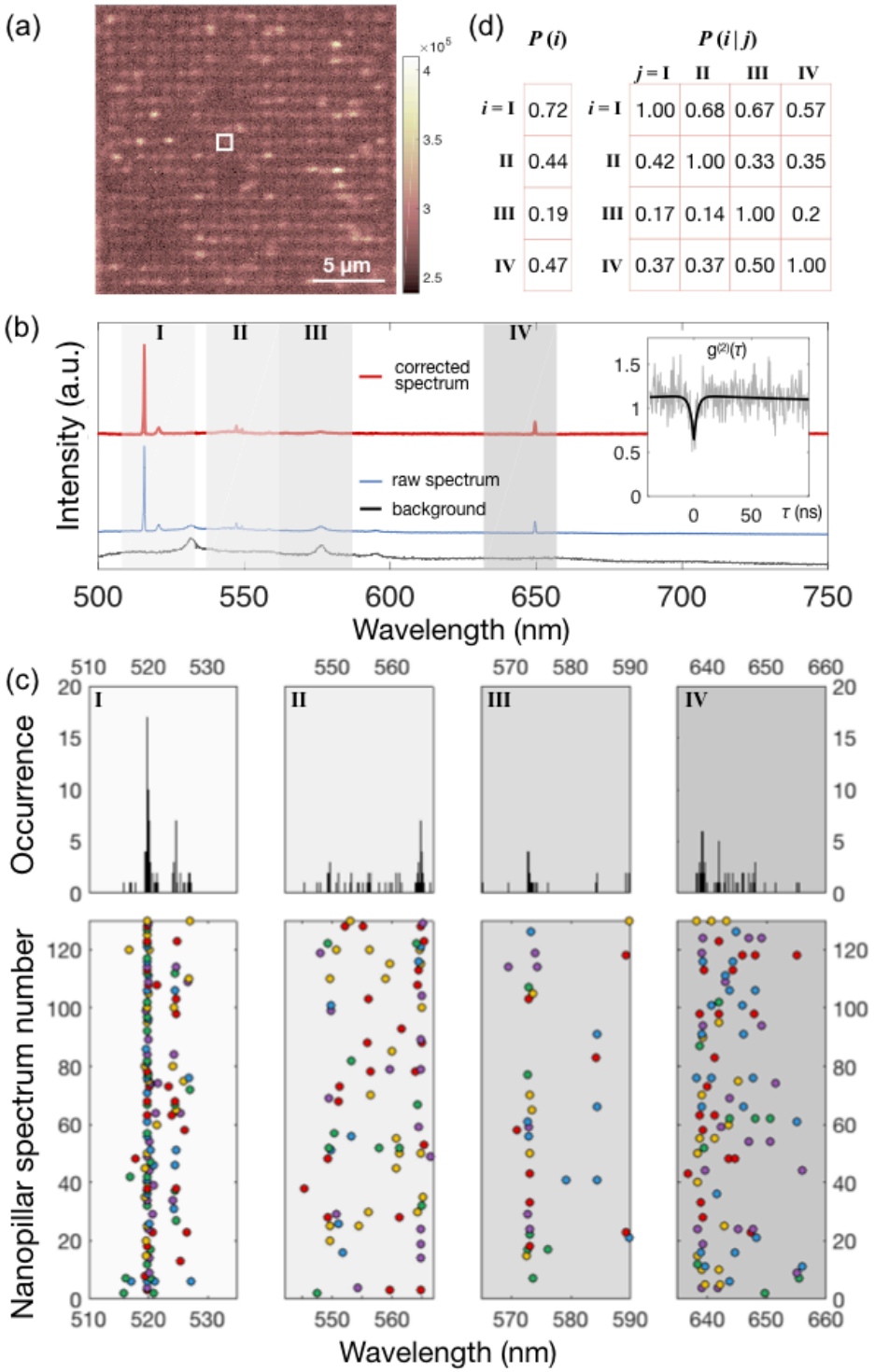

Figure 4: Cryogenic (4 K) emitter characterization. (a) Confocal scan of Pb-related emitters in nanopillars. Colorbar: counts per second. White box indicates a single emitter of interest as described below. (b) Emission spectrum of boxed emitter. Four regions with observed emission lines are shaded and labeled. Inset: antibunched emission with $g^2(0) = 0.52$ ($g^2(0) = 0.28$ after background correction) and antibunching time constant of 3.0 ns. (c) Summary of photoluminescence spectra from 129 pillars. Circles indicate the center of an observed emission peak, and colors correspond to individual pillars horizontally across spectral regions. Top:

histogram of emission peak locations. (d) Overall and conditional probabilities for the observation of emission in each region.

Figure 4 summarizes fluorescence spectroscopy of Pb-related emitters in these nanopillars, acquired using a cryogenic confocal microscope (NA = 0.9) at a temperature of 4 K. Figure 4a shows a representative confocal scan of a 20 x 20 array of 225 nm diameter pillars using an excitation laser at 450 nm (750 μW). Bright spots corresponding to emitters in individual nanopillars are clearly visible. We observe a photon count rate of ~5000 counts per second at a pump power of 750 μW; but we were unable to saturate the emitter due to limitations on the accessible excitation power in our setup. Figure 4b shows a representative spectrum from the pillar indicated by the white box in Figure 4a. This pillar contains a single emitter (red curve) as verified by second-order autocorrelation measurements (see inset of 4b). After correcting for the observed sample-independent background (gray), we measure $g^{(2)}(0) = 0.28$ including all sample-dependent background, indicating quantum emission from a single emitter. Additional spectra from the 225 nm diameter posts are displayed in the Supplemental Materials[36].

Figure 4c shows a statistical investigation of Pb-related emitter spectral properties. We analyze fluorescence from the 133 brightest nanopillars within the four distinct spectral regions indicated as I-IV in Figure 4b. The circles in Figure 4c indicate the fitted location of emission peaks observed for each nanopillar in the dataset. Binning the peak locations creates an inhomogeneous spectrum of Pb-related emitters (Figure 4c, top). Finally, we calculate the overall ($P(i)$) and conditional ($P(i \mid j)$) probabilities of observing an emission line in a given region (Figure 4d). We do not observe any significant correlation between emission regions, with $P(i) \approx P(i|j)\ \forall\ i \neq j$.

We tentatively attribute the lines in Regions III and IV (575 and 640 nm) to neutral and negatively charged NV centers[37], respectively, which are formed in the implantation process from residual nitrogen atoms naturally present in the diamond. We note that many of these emitters have large shifts from the unstrained NV ZPL position, which could be due to large strains induced by Pb implantation. The presence of peaks in Region III (NV^0) and Region IV (NV^-) indicates that the charge environment of the implanted layer is not uniform. In addition, the lack of correlation between the regions shows that the NVs that do exist are preferentially in a single charge state, unlike reported photochromic NV centers[38,39] in similar ultrapure type-IIa diamond without Pb implant.

The emission lines in Region I have not been previously reported, and we attribute them to Pb-related defect centers. The observed inhomogeneous linewidths (0.172 nm and 0.134 nm) of the prominent doublet at 520 nm in Region I are broadened between sites. However, individual diffraction-limited spots do display lines narrower than our spectrometer-limited resolution of 0.1 nm. The measured splitting of the Region I peaks, 5.2 nm (5.7 THz), is greater than that measured for the ground state of the SiV[26], GeV[17], and SnV[18].

Discussion

The theoretically calculated and experimentally measured PbV-emitter ZPL are in relatively good agreement, with the experimentally measured ZPL doublet at 520 nm close to the simulated 517 nm. Theory predicts a four-level state structure which , which points to split peaks in the emission spectra. At 4 K, we find that the ground-state splitting is 5.7 THz, which is relatively close to the theoretical predicted value of 7.25 THz. The discrepancy between these values is likely due to the theoretical value being too large (see Section 2). However, emission associated with the upper excited state, which is expected to be present at higher temperatures, was not conclusively observed in experiment. These transitions could be outside of the

accessible spectral range (> 500 nm) in our measurement setup. In addition, the large predicted excited state splitting of 260 meV would lead to a very small upper excited state population after equilibration with the lower excited state, in turn producing little fluorescence emission into these transitions. Nonetheless, the line featured at 520 nm is prominent and has yet to be reported in diamond. For this reason, we assign this peak to the PbV color center.

In addition to this pronounced line, cryogenic spectroscopy revealed other spectral features. There are several possible causes for these additional lines. SnV centers produced by implantation show a broad (> 30 nm) inhomogeneous distribution[18,19] following annealing at temperatures below 2000 °C, including several peaks attributed to intermediate defect states. These states are eliminated upon high-pressure high-temperature annealing[18], which has been shown to reduce strain in the diamond lattice in addition to allowing defects to relax to lower-energy configurations. Pb implantation produces more vacancies per ion than Sn and in a smaller volume, and thus can significantly alter the lattice during implantation. Resulting intermediate defect states and highly strained local environments could thus account for the observed emission lines. Finally, other Pb-vacancy configurations, such as a triple-vacancy or other higher-order aggregates, may be produced

The charge stability of the PbV defect is another potential cause of additional spectral features. We theoretically predict a charge transition level to be 2.71 eV above the valence band maximum. This suggests that photoionization could contribute to spectra by illumination into the phonon sideband under our pump at 450 nm (2.76 eV), as seen with NV[40,41] and SiV centers[42]. We observed fluorescence instability in some centers under blue illumination[36], which could indicate the presence of an alternate charge state. Additionally, other spectral features are observed in fluorescence under 532 nm illumination (appearance of lines around 590 and 715 nm,[36]t). Future measurements, such as photoluminescence excitation spectroscopy under varying electromagnetic and strain fields, will be required to fully determine the optical properties and electronic structure of the observed Pb-related emitters.

In conclusion, we have shown quantum emission related to Pb defects in diamond. We observe antibunched emission near 520 nm, which agrees with first-principle calculations predicting a stable, negatively-charged split-vacancy PbV center. Importantly, the ground state splitting of 5.7 THz far exceeds that for other group IV-vacancy emitters (SiV, GeV, and SnV). This splitting is in rough agreement with theory and promises long spin coherence at elevated temperatures, which is of central importance for quantum memories in proposed quantum networks and modular quantum computing schemes.

After submission of this manuscript, we became aware of an ArXiV posting[43] that also describes photoluminescence from lead-related emitters. That PL data qualitatively agrees with our findings in Regions II, III and IV. Ref 42. does not reproduce the lines we see in Region I, potentially because of different optical excitation conditions at 405 and 514 nm excitation wavelengths as compared to our use of 450 nm.

Acknowledgements
M.T. acknowledges support by an appointment to the Intelligence Community Postdoctoral Research Fellowship Program at MIT, administered by Oak Ridge Institute for Science and Education through an interagency agreement between the U.S. Department of Energy and the Office of the Director of National Intelligence. N.H.W is supported in part by the Army Research Laboratory Center for Distributed Quantum Information (CDQI). K.C.C. acknowledges funding support by the National Science Foundation Graduate Research Fellowships Program (GRFP).

J.F. acknowledges financial support from the Deutsche Forschungsgemeinschaft (DFG) under Contract No. FL 997/1-1. E.B. was supported by a NASA Space Technology Research Fellowship. D.E. and experiments were supported in part by the STC Center for Integrated Quantum Materials (CIQM), NSF Grant No. DMR-1231319. This research used resources of the National Energy Research Scientific Computing Center, a DOE Office of Science User Facility supported by the Office of Science of the U.S. Department of Energy, as well as resources at the Research Computing Group at Harvard University.

Bibliography

[1] D.D. Awschalom, L.C. Bassett, A.S. Dzurak, E.L. Hu, and J.R. Petta, Science **339**, 1174 (2013).
[2] M. Atatüre, D. Englund, N. Vamivakas, S.-Y. Lee, and J. Wrachtrup, Nature Reviews Materials (2018).
[3] M.H. Abobeih, J. Cramer, M.A. Bakker, N. Kalb, D.J. Twitchen, M. Markham, and T.H. Taminiau, arXiv [quant-Ph] (2018).
[4] E. Togan, Y. Chu, A.S. Trifonov, L. Jiang, J. Maze, L. Childress, M.V.G. Dutt, A.S. Sørensen, P.R. Hemmer, A.S. Zibrov, and M.D. Lukin, Nature **466**, 730 (2010).
[5] N. Kalb, A.A. Reiserer, P.C. Humphreys, J.J.W. Bakermans, S.J. Kamerling, N.H. Nickerson, S.C. Benjamin, D.J. Twitchen, M. Markham, and R. Hanson, Science **356**, 928 (2017).
[6] S. Pezzagna, D. Rogalla, D. Wildanger, J. Meijer, and A. Zaitsev, New J. Phys. **13**, 035024 (2011).
[7] D. Riedel, I. Söllner, B.J. Shields, S. Starosielec, P. Appel, E. Neu, P. Maletinsky, and R.J. Warburton, Phys. Rev. X **7**, 031040 (2017).
[8] A. Faraon, C. Santori, Z. Huang, V.M. Acosta, and R.G. Beausoleil, Phys. Rev. Lett. **109**, 033604 (2012).
[9] L. Li, T. Schröder, E.H. Chen, M. Walsh, I. Bayn, J. Goldstein, O. Gaathon, M.E. Trusheim, M. Lu, J. Mower, M. Cotlet, M.L. Markham, D.J. Twitchen, and D. Englund, Nat. Commun. **6**, 6173 (2015).
[10] E. Neu, C. Hepp, M. Hauschild, S. Gsell, M. Fischer, H. Sternschulte, D. Steinmüller-Nethl, M. Schreck, and C. Becher, New J. Phys. **15**, 043005 (2013).
[11] R.E. Evans, A. Sipahigil, D.D. Sukachev, A.S. Zibrov, and M.D. Lukin, Phys. Rev. Applied **5**, 044010 (2016).
[12] A. Sipahigil, K.D. Jahnke, L.J. Rogers, T. Teraji, J. Isoya, a. S. Zibrov, F. Jelezko, and M.D. Lukin, Phys. Rev. Lett. **113**, 113602 (2014).
[13] L.J. Rogers, K.D. Jahnke, M.W. Doherty, A. Dietrich, L.P. McGuinness, C. Müller, T. Teraji, H. Sumiya, J. Isoya, N.B. Manson, and F. Jelezko, Phys. Rev. B: Condens. Matter Mater. Phys. **89**, 235101 (2014).
[14] D.D. Sukachev, A. Sipahigil, C.T. Nguyen, M.K. Bhaskar, R.E. Evans, F. Jelezko, and M.D. Lukin, Phys. Rev. Lett. **119**, 223602 (2017).
[15] G. Thiering and A. Gali, Phys. Rev. X **8**, 021063 (2018).
[16] M.K. Bhaskar, D.D. Sukachev, A. Sipahigil, R.E. Evans, M.J. Burek, C.T. Nguyen, L.J. Rogers, P. Siyushev, M.H. Metsch, H. Park, F. Jelezko, M. Lončar, and M.D. Lukin, Phys. Rev. Lett. **118**, 223603 (2017).
[17] P. Siyushev, M.H. Metsch, A. Ijaz, J.M. Binder, M.K. Bhaskar, D.D. Sukachev, A. Sipahigil, R.E. Evans, C.T. Nguyen, M.D. Lukin, P.R. Hemmer, Y.N. Palyanov, I.N. Kupriyanov, Y.M. Borzdov, L.J. Rogers, and F. Jelezko, Phys. Rev. B Condens. Matter **96**, 081201 (2017).
[18] T. Iwasaki, Y. Miyamoto, T. Taniguchi, P. Siyushev, M.H. Metsch, F. Jelezko, and M. Hatano, Phys. Rev. Lett. **119**, 253601 (2017).
[19] S.D. Tchernij, T. Herzig, J. Forneris, J. Küpper, S. Pezzagna, P. Traina, E. Moreva, I.P.

Degiovanni, G. Brida, N. Skukan, M. Genovese, M. Jakšić, J. Meijer, and P. Olivero, ACS Photonics **4**, 2580 (2017).
[20] C. Wang, C. Kurtsiefer, H. Weinfurter, and B. Burchard, J. Phys. B At. Mol. Opt. Phys. **39**, 37 (2005).
[21] Y.N. Palyanov, I.N. Kupriyanov, Y.M. Borzdov, and N.V. Surovtsev, Sci. Rep. **5**, 14789 (2015).
[22] P. Giannozzi, O. Andreussi, T. Brumme, O. Bunau, M. Buongiorno Nardelli, M. Calandra, R. Car, C. Cavazzoni, D. Ceresoli, M. Cococcioni, N. Colonna, I. Carnimeo, A. Dal Corso, S. de Gironcoli, P. Delugas, R.A. DiStasio, A. Ferretti, A. Floris, G. Fratesi, G. Fugallo, R. Gebauer, U. Gerstmann, F. Giustino, T. Gorni, J. Jia, M. Kawamura, H.-Y. Ko, A. Kokalj, E. Küçükbenli, M. Lazzeri, M. Marsili, N. Marzari, F. Mauri, N.L. Nguyen, H.-V. Nguyen, A. Otero-de-la-Roza, L. Paulatto, S. Poncé, D. Rocca, R. Sabatini, B. Santra, M. Schlipf, A.P. Seitsonen, A. Smogunov, I. Timrov, T. Thonhauser, P. Umari, N. Vast, X. Wu, and S. Baroni, J. Phys. Condens. Matter **29**, 465901 (2017).
[23] P. Giannozzi, S. Baroni, N. Bonini, M. Calandra, R. Car, C. Cavazzoni, D. Ceresoli, G.L. Chiarotti, M. Cococcioni, I. Dabo, A. Dal Corso, S. de Gironcoli, S. Fabris, G. Fratesi, R. Gebauer, U. Gerstmann, C. Gougoussis, A. Kokalj, M. Lazzeri, L. Martin-Samos, N. Marzari, F. Mauri, R. Mazzarello, S. Paolini, A. Pasquarello, L. Paulatto, C. Sbraccia, S. Scandolo, G. Sclauzero, A.P. Seitsonen, A. Smogunov, P. Umari, and R.M. Wentzcovitch, J. Phys. Condens. Matter **21**, 395502 (2009).
[24] D.R. Hamann, Phys. Rev. B Condens. Matter **88**, 085117 (2013).
[25] J.P. Perdew, K. Burke, and M. Ernzerhof, Phys. Rev. Lett. **77**, 3865 (1996).
[26] C. Hepp, T. Müller, V. Waselowski, J.N. Becker, B. Pingault, H. Sternschulte, D. Steinmüller-Nethl, A. Gali, J.R. Maze, M. Atatüre, and C. Becher, Phys. Rev. Lett. **112**, 036405 (2014).
[27] J. Heyd, G.E. Scuseria, and M. Ernzerhof, J. Chem. Phys. **118**, 8207 (2003).
[28] R.O. Jones and O. Gunnarsson, Rev. Mod. Phys. **61**, 689 (1989).
[29] F.S. Ham, Phys. Rev. **138**, A1727 (1965).
[30] C.D. Clark, H. Kanda, I. Kiflawi I., and G. Sittas, Phys. Rev. B Condens. Matter **51**, 16681 (1995).
[31] R. Sundararaman, K. Letchworth-Weaver, K.A. Schwarz, D. Gunceler, Y. Ozhabes, and T.A. Arias, SoftwareX **6**, 278 (2017).
[32] A.M. Brown, R. Sundararaman, P. Narang, W.A. Goddard 3rd, and H.A. Atwater, ACS Nano **10**, 957 (2016).
[33] A.M. Brown, R. Sundararaman, P. Narang, W.A. Goddard, and H.A. Atwater, Phys. Rev. B Condens. Matter **94**, 075120 (2016).
[34] J.F. Ziegler, M.D. Ziegler, and J.P. Biersack, Nucl. Instrum. Methods Phys. Res. B **268**, 1818 (2010).
[35] C. Uzan-Saguy, C. Cytermann, R. Brener, V. Richter, M. Shaanan, and R. Kalish, Appl. Phys. Lett. **67**, 1194 (1995).
[36] See Supplemental Material at [URL will be inserted by publisher] for information on experimental methods and sample preparation, PL spectra under 532 illumination, and high-resolution and temperature-dependent spectra.
[37] M.W. Doherty, N.B. Manson, P. Delaney, F. Jelezko, J. Wrachtrup, and L.C.L. Hollenberg, Phys. Rep. **528**, 1 (2013).
[38] T. Gaebel, M. Domhan, C. Wittmann, I. Popa, F. Jelezko, J. Rabeau, A. Greentree, S. Prawer, E. Trajkov, P.R. Hemmer, and J. Wrachtrup, Appl. Phys. B **82**, 243 (2005).
[39] N. Aslam, G. Waldherr, P. Neumann, F. Jelezko, and J. Wrachtrup, New J. Phys. **15**, 013064 (2013).
[40] K. Beha, A. Batalov, N. Manson, R. Bratschitsch, and A. Leitenstorfer, Phys. Rev. Lett. **109**, 1 (2012).
[41] P. Siyushev, H. Pinto, M. Vörös, A. Gali, F. Jelezko, and J. Wrachtrup, Phys. Rev. Lett. **110**,

167402 (2013).
[42] U.F.S. D'Haenens-Johansson, a. M. Edmonds, B.L. Green, M.E. Newton, G. Davies, P.M. Martineau, R.U. a. Khan, and D.J. Twitchen, Phys. Rev. B: Condens. Matter Mater. Phys. **84**, 245208 (2011).
[43] S. Ditalia Tchernij, T. Lühmann, J. Forneris, T. Herzig, J. Küpper, A. Damin, S. Santonocito, P. Traina, E. Moreva, F. Celegato, S. Pezzagna, I.P. Degiovanni, M. Jakšić, M. Genovese, J. Meijer, and P. Olivero, arXiv [cond-Mat.mtrl-Sci] (2018).